Princeton Plasma Physics Laboratory

PPPL-4118
PPPL-4118

Electron Cross-field Transport in a Miniaturized Cylindrical Hall Thruster

Artem Smirnov, Yevgeny Raitses,
and Nathaniel J. Fisch

October 2005

PPPL
PRINCETON PLASMA PHYSICS LABORATORY

Prepared for the U.S. Department of Energy under Contract DE-AC02-76CH03073.

Princeton Plasma Physics Laboratory
Report Disclaimers

Full Legal Disclaimer

Trademark Disclaimer

PPPL Report Availability

Princeton Plasma Physics Laboratory

This report is posted on the U.S. Department of Energy's Princeton Plasma Physics Laboratory Publications and Reports web site in Fiscal Year 2006.

The home page for PPPL Reports and Publications is:

http://www.pppl.gov/pub_report/

Office of Scientific and Technical Information (OSTI):

Available electronically at: http://www.osti.gov/bridge.

Available for a processing fee to U.S. Department of Energy and its contractors, in paper from:

U.S. Department of Energy
Office of Scientific and Technical Information
P.O. Box 62
Oak Ridge, TN 37831-0062

Telephone: (865) 576-8401

Fax: (865) 576-5728

E-mail: reports@adonis.osti.gov

Electron Cross-Field Transport in a Miniaturized Cylindrical Hall Thruster

Artem Smirnov*, *Student member, IEEE,*

Yevgeny Raitses, *Member, IEEE,*

and Nathaniel J. Fisch.

Princeton University Plasma Physics Laboratory, P.O. Box 451, Princeton, New Jersey 08543

ABSTRACT

Conventional annular Hall thrusters become inefficient when scaled to low power. Cylindrical Hall thrusters, which have lower surface-to-volume ratio, are more promising for scaling down. They presently exhibit performance comparable with conventional annular Hall thrusters. The present paper gives a review of the experimental and numerical investigations of electron cross-field transport in the 2.6 cm miniaturized cylindrical Hall thruster (100 W power level). We show that, in order to explain the discharge current observed for the typical operating conditions, the electron anomalous collision frequency ν_B has to be on the order of the Bohm value, $\nu_B \approx \omega_c/16$. The contribution of electron-wall collisions to cross-field transport is found to be insignificant. The optimal regimes of thruster operation at low background pressure (below 10^{-5} Torr) in the vacuum tank appear to be different from those at higher pressure (~10^{-4} Torr).

* asmirnov@pppl.gov

I. INTRODUCTION

The Hall thruster [1] is a well-studied electric propulsion device at intermediate to high power, but it appears to be promising also for relatively low power propulsion on near-Earth missions [2], such as orbit transfer and repositioning. In a conventional Hall thruster, the plasma discharge is sustained in the axial electric (**E**) and radial magnetic (**B**) fields applied in an annular channel. The magnetic field is large enough to lock the electrons in the azimuthal **E**×**B** drift, but small enough to leave the ion trajectories almost unaffected. A large fraction of the discharge electrons is emitted by an external cathode. Electron cross-field diffusion provides the necessary current to sustain the discharge. The thrust is generated in reaction to the axial electrostatic acceleration of ions. Ions are accelerated in a quasineutral plasma, so that no space-charge limitation is imposed on the achievable current and thrust densities. Conventional Hall thrusters designed for operation in 600–1000 W power range have outer channel diameter about 10 cm, maximal value of the magnetic field about 100–200 G, and applied discharge voltage U_d =300V.

The thruster efficiency is defined as $\eta=T^2/2\mu P$, where T is the generated thrust, μ is the supplied propellant flow rate, and P is the applied electric power. The efficiency of the state-of-the-art kilowatt and subkilowatt conventional Hall thrusters is about 50–60% [1], [3]. The efficiency can be conveniently factorized as:

$$\eta \approx \frac{I_i M}{e\mu} \times \frac{I_i}{I_i + I_e} \times \alpha \,, \tag{1}$$

where M is a mass of a propellant gas atom, e is the electron charge, I_i and I_e are the electron and ion currents, respectively, and α is the efficiency of ion acceleration. The first fraction in the right hand side of Eq. (1), the so-called propellant utilization, is a measure of how effectively the supplied propellant gas is ionized in the discharge, whereas the second fraction, the so-called current utilization, determines how effectively the electron transport to the anode is suppressed by the applied magnetic field. With all other parameters held constant, the thruster efficiency decreases with increasing electron current. Understanding of the mechanisms of electron transport in the discharge is, therefore, essential for the development of higher efficiency thrusters.

The electrons in Hall thrusters exhibit anomalous cross-field transport: The electron conductivity across the magnetic field is larger than that predicted by the classical electron-atom collision rate [1], [4]. It is believed that two collisional processes contribute to the conductivity enhancement in Hall thrusters: i) electron scattering in electric field fluctuations (anomalous or 'Bohm' diffusion [4]), and ii) the electron-wall collisions (the near-wall conductivity [5], [6]). The electron-wall interaction plays also a very important role by shaping the electron distribution function (EDF) in the thruster channel. In Hall discharge simulations, in order to account for an enhanced electron cross-field transport, the two non-classical conductivity mechanisms are usually incorporated in models in one or another parametric way. In fluid and hybrid fluid-particle models, some investigators impose the anomalous Bohm conductivity inside the channel [7]-[9], while others use only the near-wall conductivity [10] or a combination of both Bohm transport and wall collisions [8]-[16]. Full particle-in-cell (PIC) simulations [17], [18] reveal turbulence increasing the cross-field transport. Some theoretical studies [19], [20] suggest that due to the non-Maxwellian shape of the EDF in a Hall thruster, electron-wall collisions do not

make a significant contribution to cross-field transport. In a 2-kW Hall thruster operated at low discharge voltage [21], in the channel region where the magnetic field was the strongest, anomalous fluctuation-enhanced diffusion was identified as the main mechanism of electron cross-field transport. It is important to emphasize here that most of investigations, which addressed the question of the electron conductivity, have been performed for kilowatt and sub-kilowatt thrusters, where the maximal magnetic field strength in the channel is about 100–200 G.

Scaling to low power Hall thrusters requires a thruster channel size to be decreased while the magnetic field must be increased inversely to the scaling factor [1]. Thus, in general, the rate of electron cross-field transport required to sustain the discharge in a low-power thruster may be different from that in kilowatt thrusters. In other types of low-temperature magnetized laboratory plasmas, variation of the electron cross-field diffusion rate with applied magnetic field B occurs indeed: For example, in [22], cross-field diffusion coefficient $D_\perp$ was observed to approach the Bohm value when B was greater than 2-3 kG, while in $B<1$ kG case $D_\perp$ was much smaller than the Bohm value.

Increasing the magnetic field while the thruster channel sizes are being reduced is technically challenging because of magnetic saturation in the miniaturized inner parts of the magnetic core. A linear scaling down of the magnetic circuit leaves almost no room for magnetic poles or for heat shields, making difficult the achievement of the optimal magnetic fields. Non-optimal magnetic fields result in enhanced electron transport, power and ion losses, heating and erosion of the thruster parts, particularly the critical inner parts of the coaxial channel and magnetic circuit.

Currently existing low-power Hall thruster laboratory prototypes with channel diameters 2–4 cm operate at 100–300 W power levels with efficiencies in the range of 10%–40% [2]. However,

further scaling of the conventional geometry Hall thruster down to sub-centimeter size results in even lower efficiencies, 6% at power level of about 100 W [23]. The low efficiency might arise from a large axial electron current, enhanced by magnetic field degradation due to excessive heating of the thruster magnets, or from a low degree of propellant ionization. Thus, miniaturizing the conventional annular Hall thruster does not appear to be straightforward.

A cylindrical Hall thruster (CHT), illustrated in Fig. 1(a), overcomes these miniaturization problems [24]. It has been studied both experimentally and theoretically [25]-[28]. The thruster consists of a boron-nitride ceramic channel, an annular anode, which serves also as a gas distributor, two electromagnetic coils, and a magnetic core. The axial electron current in a CHT can be reduced by the magnetic field with an enhanced radial component and/or by the strong magnetic mirror in the cylindrical part of the channel. The magnetic field lines intersect the ceramic channel walls. The electron drifts are closed, with the magnetic field lines forming equipotential surfaces, with $E=-\upsilon_e \times B$. Ion thrust is generated by the axial component of the Lorentz force, proportional to the radial magnetic field and the azimuthal electron current.

The cylindrical channel features a short annular region and a longer cylindrical region. The length of the annular region is selected to be approximately equal to an ionization mean free path of a neutral atom. Compared to a conventional geometry (annular) Hall thruster, the CHT has lower surface-to-volume ratio and, therefore, potentially smaller wall losses in the channel. Having potentially smaller wall losses in the channel, a CHT should suffer lower erosion and heating of the thruster parts, particularly the critical inner parts of the channel and magnetic circuit. This makes the concept of a CHT promising for low-power applications.

In contrast to the conventional annular geometry, in the cylindrical geometry the axial potential distribution is critical for electron confinement. This is because there is now a large

axial gradient to the magnetic field over the cylindrical part of the channel, which means that electrons drift outwards through the $\mu_e \nabla B$ force, even as they drift azimuthally around the cylinder axis. In the absence of an axial potential, the electrons would simply mirror out of the region of high magnetic field. The axial potential that accelerates ions outwards, now also plays an important role in confining electrons within the thruster.

A relatively large 9 cm diameter version of the cylindrical thruster, operated in the subkilowatt power range [24], and miniaturized 2.6 cm [25] and 3 cm diameter CHTs [29], [30], operated in the power range 50–300 W, exhibit performance comparable with that of the conventional state-of-the-art annular Hall thrusters of the same size. In Ref. 27 the plasma potential, electron temperature, and plasma density distributions were measured inside the 2.6 cm CHT. It was found that even though the radial component of the magnetic field has a maximum inside the annular part of the CHT, the larger fraction of the applied voltage is localized in the cylindrical region. A significant potential drop was also observed in the plume. Ion acceleration in the CHT is expected to occur predominantly in the longitudinal direction and towards the thruster axis. Therefore, the CHT, having lower surface-to-volume ratio as compared with conventional Hall thrusters, may suffer lower erosion of the channel walls and have a longer lifetime.

In recent work [28], electron cross-field transport in a 2.6 cm miniaturized cylindrical Hall thruster was studied through the analysis of experimental data and Monte Carlo simulations of electron dynamics in the thruster channel. The numerical model takes into account elastic and inelastic electron collisions with atoms, electron-wall collisions, including secondary electron emission, and Bohm diffusion. It was shown that in the typical operating regime the electron

anomalous collision frequency ν_B was of the order of the Bohm value, $\nu_B \approx \omega_c/16$. The contribution of electron-wall collisions to cross-field transport was found to be insignificant.

The present paper gives a review of the experimental and numerical investigations of electron cross-field transport in the 2.6 cm CHT and reports a few recent experimental results that suggest directions for further studies.

This article is organized as follows: In Sec. II, the main features of the 2.6 cm CHT are presented and the experimental results, obtained in the vacuum facility with a relatively high background pressure, are reviewed. Section III gives a description of the developed MC code and outlines the key results of the numerical simulations. We discuss the electron cross-field transport in Sec. IV. In Sec. V, a few recent experimental results, obtained at low background pressure, are presented, and their implications are discussed. In Sec. VI, we summarize our main conclusions.

II. EXPERIMENTS

The results of comprehensive experimental investigations of the 2.6 cm CHT are given in Refs. 25-29. Experiments described in this section were performed in the Small Hall Thruster facility at Princeton Plasma Physics Laboratory (PPPL).

The 2.6 cm CHT, shown in Fig. 1(b), was scaled down from the 9 cm CHT to operate at about 200 W power level. The total length of the channel is 2.2 cm, the annular region is approximately 0.6 cm long. The outer and the inner diameters of the channel are 2.6 cm and 1.4 cm, respectively. The overall diameter and the thruster length are both 7 cm.

The magnetic field profiles in the 2.6 cm CHT are shown in Fig. 2(a). The radial component B_r of the magnetic field reaches its maximum near the anode and then reduces towards the channel exit. Although the axial component B_z is also strong, the magnetic field in the annular part of the channel is predominantly radial, the average angle between the field line and the normal to the walls is about 30° [see Fig. 2(b)]. Magnetic field has a mirror-type structure near the thruster axis, with the maximum B ~ 1400 G at the central ceramic piece wall. Due to the mirroring effect of the magnetic field in the cylindrical part of the channel [see Fig. 2(b)], most of the electrons injected from the cathode are reflected from the region of strong B field, and move in the downstream direction. Upon crossing the thruster exit plane and entering the plume plasma, the electrons become unmagnetized and face the potential drop of about 100 V, which reflects them back into the thruster. Thus, most of the electrons injected from the cathode to the CHT appear to be confined in a hybrid trap formed by the magnetic mirror and by the plume potential drop. Diffusion of these electrons across the magnetic field occurs on a time scale much larger than the bounce time in the trap [28].

The typical discharge parameters for the 2.6 cm CHT are: Xe flow rate μ=0.4 mg/s, discharge voltage U_d=250 V, discharge current $I_d \approx$ 0.6 A. Under such conditions, the background gas pressure in the PPPL Small Hall Thruster facility is about 7×10^{-5} Torr, the propellant utilization in the 2.6 cm CHT is about 1, and the current utilization is approximately equal to 0.5 [25]. In practice, for the given propellant flow rate, discharge voltage, and background gas pressure, the discharge current is minimized by varying the currents in the magnetic coils. This procedure, which appears to be customary for the annular thrusters, is based on the assumption that, near the discharge current minimum, the variation of the magnetic field affects mainly the electron current to the anode but not the ion current. Thus, the thruster

efficiency is maximized by decreasing the discharge current while keeping the generated thrust nearly constant. As shown in Sec. V, this approach is valid for the CHTs operated at a low background gas pressure (in the 10^{-6} Torr range). However, in the relatively high background pressure of the Small Hall Thruster facility (~ 10^{-4} Torr), the reduction of the discharge current in certain magnetic field configurations may be due to the suppression of the background gas ionization. Nonetheless, the operating regime considered in Sec. II-IV is a typical one for the vacuum environment of the Small Hall Thruster facility.

The distribution of plasma potential ϕ, electron temperature T_e, and plasma density N_e inside the 2.6 cm CHT was studied by means of stationary and movable floating emissive and biased Langmuir probes [28]. The probe setup used in the experiments is shown in Fig. 2(b). Measurements were done at the outer channel wall (at four axial locations: z = 5, 10.3, 13.5, and 22 mm), as well as at the thruster axis. The results of the probe measurements are shown in Fig. 3. The potential drop in the 2.6 cm CHT is localized mainly in the cylindrical part of the channel and beyond the thruster exit, in the plume. The potential variation along the thruster axis between the central ceramic piece and the channel exit is insignificant. Its maximum possible value is within the data spread of the measurements, which is about 25 V. Much larger potential drops along the magnetic field lines were observed in the end-Hall ion source [31], which has a mirror-type magnetic field distribution similar to that in the central part of the CHT.

Due to a rather large uncertainty of the plasma density measurements, it was possible to determine only the interval, in which the real value of N_e was located. The variation bars in Fig. 3(c) span between the upper and the lower estimates of N_e obtained in the experiments. Due to the reasons discussed in detail in Ref. 27, the real values of the plasma density are believed to be closer to the upper bounds of the corresponding intervals. The plasma density in the 2.6 cm CHT

has a prominent peak at the thruster axis: N_e at the axis is 4–8 times larger than in the annular part of the channel. This density elevation at the thruster axis should be, in fact, common to all scaled down Hall thrusters and might lead to the enhanced erosion of the tip of the central ceramic piece.

III. NUMERICAL SIMULATIONS

The MC code, developed to study the electron dynamics in the thruster channel, is described in detail elsewhere [28]. In the present paper, we only outline the main code's features and show the major results of the numerical simulations.

A. Modeling approach and assumptions

The MC code in the present realization is used to simulate the charged particles dynamics in the channel of the 2.6 cm CHT. The particle trajectories are traced in the given electric and magnetic fields, which are assumed to be azimuthally symmetric. The magnetic field distribution for a given arrangement of the magnetic circuit is simulated using the commercially available Field Precision software [32].

The electric field distribution is obtained from the experiments assuming that the magnetic field surfaces are equipotential. We assign the measured potential values to the magnetic field lines sampled by the corresponding probes [see Fig. 2(b)]. Between the locations of the probes plasma potential $\phi(z,R)$ is assumed to vary linearly with magnetic flux function $\psi(z,R)$, $\phi(z,R) \propto \psi(z,R)$. The anode's surface is equipotential with ϕ=250 V. As suggested by the measurements,

the magnetic field line at the thruster axis is assumed to be equipotential as well, and is assigned the potential of 100 V. The sheath potential drop is assumed to be concentrated in the infinitely thin layer near the walls. For the results of measurements shown in Fig. 3, the resultant "tailored" plasma potential profile is plotted in Fig. 4. All numerical simulations were done for this distribution of the plasma potential.

In the MC simulations charged particle trajectories are integrated in 3D-3υ (three dimensions in configuration space, three dimensions in velocity space). Newton's equations of motion are resolved using a modification of the explicit leap-frog scheme by Boris [33]. The time step of integration $\Delta t=0.1/\omega_c$ was used in simulations, where ω_c is the particle gyrofrequency (for electrons, $\Delta t\sim 3\times10^{-12}$s).

We apply the MC technique [34] to simulate electron collisions, which include collisions with neutral Xe atoms (elastic scattering, excitation, and single ionization), with channel walls (attachment, backscattering, and secondary electron emission [SEE]), and with electric field fluctuations (anomalous or "Bohm" diffusion). For simplicity, the neutral gas density N_a is assumed to be uniform in the entire channel volume, and the near-wall sheath potential drop ϕ_{sh} is assumed to be constant along all the channel walls. To treat MC collisions, the numerically efficient null-collision method [30] is implemented in the code.

We imposed the anomalous Bohm conductivity inside the channel in order to account for fluctuation-enhanced electron transport. It was assumed that electrons scatter primarily in the azimuthal fluctuations of the electric field. When an electron undergoes a collision with the electric field fluctuation, the perpendicular, with respect to **B**, electron velocity component is assumed to scatter isotropically. The parallel velocity component does not change. Thus, the guiding center of the electron orbit gets a random shift in the plane perpendicular to **B** on the

order of the electron gyroradius. The frequency of Bohm diffusion collisions is assumed to be $\nu_B = \kappa_B \omega_c/16$, where κ_B is a fitting parameter that does not depend on the electron energy. Using the customary approach, we introduce one fitting parameter, κ_B, which is applied to calculation of the anomalous collision frequency in the entire discharge volume. However, in reality the effective κ_B may vary across the magnetic field [21].

It is worth mentioning that for kilowatt and subkilowatt Hall thrusters most of the models that impose Bohm conductivity in the channel show that the best agreement between the experimental and simulated data is achieved when κ_B is less than one, on the order of 0.1–0.4 [8], [9], [11]-[16].

In the electron transport simulations, primary electrons injected from the cathode are assumed to have monoenergetic distribution with ε=20 eV. Similar energy of electrons injected from the cathode was observed in a low-power conventional Hall thruster [35]. The primary electrons are launched at the thruster exit, with a uniform distribution of the electron flux across the channel cross section. The electrons are followed successively one after another until both primary electrons and secondary ones (the latter being generated due to ionization and secondary electron emission from the walls), either reach the anode or get attached to the walls. Electron distribution function (EDF) is determined in z-R-ε phase space using the approach developed by Boeuf and Marode [36]. Electron density and effective electron temperature are determined as the corresponding moments of the EDF.

B. Numerical results

The main objective of the performed numerical simulations was to determine what rate of electron cross-field diffusion could explain the observed discharge current. We performed the parametric study of the dependency of plasma parameters distribution on the electron cross-field conductivity. Numerical simulations were carried out for four different values of κ_B, with N_a and ϕ_{sh} chosen according to the experimental constraints [28]. The main results obtained in the simulations can be summarized as follows.

The distributions of the electron density N_e and effective electron temperature T_{eff} obtained in simulations are shown in Fig. 5. Note that the maximum electron density is achieved in the annular part of the channel. Although there is a slight elevation of N_e at the thruster axis, its value, as opposed to the results of the experiments, is lower than the density in the annular part of the channel. The plasma density spike observed at the thruster axis [see Fig. 3(c)] might be due to the convergent ion flux [37]. When κ_B is varied, the distribution of the electron density in the channel remains similar to that shown in Fig. 5(a), with the characteristic magnitude of N_e decreasing when κ_B is increased. For different values of κ_B, the distributions of T_{eff} remain very similar to each other.

When the parameter κ_B is increased, the electron density required to conduct the observed discharge current becomes smaller. This fact is illustrated in Fig. 6, where the axial profiles of N_e near the outer channel wall are plotted for different values of κ_B. As the rate of cross-field electron diffusion approaches the Bohm value κ_B=1 [38], the electron density at z=5 mm and 13.5 mm gets almost equal to the measured plasma density. As mentioned herein, the real values of the plasma density are believed to be closer to the upper bounds of the corresponding uncertainty bars in Fig. 6. Even though the match between the measured and simulated values of N_e is not perfect, the trend of N_e dependency on κ_B is evident.

The present model is not expected to give a correct quantitative description of the EDF variation along the thruster channel. However, the general shape of the EDF obtained in our simulations appears to be in a good qualitative agreement with the results of work [20], where the EDF in the Hall thruster channel was determined by solving the electron Boltzman equation.

A typical EDF in the annular part of the channel is shown in Fig. 7. The EDF averaging is performed in order to get statistically more ample phase space data. As can be concluded from Fig. 7, electron-wall collisions deplete the tail of the EDF. The resultant shape of the EDF appears to be bi-Maxwellian. In the given distribution of electric field, Bohm parameter κ_B governs the rate of electron thermal energy pumping. As κ_B (and, consequently, ν_B) decreases, the tail of the distribution function gradually weakens. For κ_B=1 (as in Fig. 7), the ratio of the bulk and the tail electron temperatures is approximately equal to 2.1. For κ_B=0.16 this ratio increases to 3.3, while the effective electron temperature remains approximately the same as in κ_B=1 case. In the cylindrical part of the channel, where the electron-wall collision frequency is smaller, the influence of the walls on the EDF shape is less pronounced.

IV. DISCUSSION

In view of Fig. 6, in order to explain the observed plasma density, the electron anomalous collision frequency ν_B should be high, on the order of the Bohm value $\nu_B \sim \omega_c/16$ (κ_B=1). This conclusion can be supported also by the following argument concerning electron current conduction in the annular part of the channel. The magnetic field in the annular part of the 2.6 cm CHT is mainly radial. The average value of the magnetic field at the median is about 650 G. At z=5 mm, where the closest to the anode probe was located in the experiments, the axial

electric field E is about 110 V/cm. We can estimate the average electron velocity in the axial direction U_e as $U_e=\kappa_B Ee/(16m\omega_c) \sim 1.06\kappa_B\times10^6$ cm/s. Now, we note that in the 2.6 cm CHT the fraction of the discharge current carried by the ions varies from essentially zero at the anode ($I_i<<I_e$) to about 0.5 at the thruster exit ($I_i\approx I_e\approx I_d/2$). Taking in to account that the overall potential drop in the annular part of the channel is not large, we conclude that the electron current in the annular part of the channel should be at least a few times larger than the ion current. Thus, in the annular part of the channel $I_e\approx I_d\approx eN_eS_aU_e$, where S_a = 3.77 cm^2 is the anode area. Therefore, we can relate the plasma density required to conduct the observed current (I_d=0.6 A) to the rate of electron cross-field transport:

$$N_e \sim \frac{9.4}{\kappa_B}\times10^{11}\ \text{cm}^{-3} \qquad (2)$$

For κ_B=1, the value of N_e acquired from this rather crude estimate, N_e = 9.4×10^{11} cm^{-3}, is in a good agreement with the result of simulations, N_e = 8.2×10^{11} cm^{-3}. More importantly, the values of N_e obtained in simulations for different values of κ_B follow $1/\kappa_B$ scaling quite well, as illustrated in Fig. 8.

It is important to mention that the value of Bohm parameter κ_B, which, for the low-power CHT, gives the best agreement between the simulations and experiments ($\kappa_B \sim 1$), is a few times larger than those obtained typically in the modeling of conventional Hall thrusters ($\kappa_B \sim 0.1 – 0.4$) [8], [9], [11]-[16]. Thus, the rate of electron fluctuation-enhanced diffusion, which is required to explain the discharge current observed in the CHT, should be higher than that in conventional Hall thrusters. The anomalous electron transport in the CHT is believed to be

induced by high-frequency plasma instabilities [39]. Interestingly, in the frequency range below ~100 kHz, the 2.6 cm CHT operates quieter than the annular Hall thruster of the same size [25].

The electron-wall collisions make an insignificant contribution to the electron current conduction, as compared with the fluctuation-induced electron scattering. For the parameters of Fig. 7, the average electron-wall collision frequency ν_{ew} is approximately equal to 1×10^7 s^{-1}, while the anomalous collision frequency averaged along the corresponding field line is about 7.2×10^8 s^{-1} [28]. At the same time, the total electron-atom collision frequency ν_{ea} is on the order of 2.4×10^7 s^{-1}. Thus, $\nu_{ew} \leq \nu_{ea} << \nu_B$. Both the electron-wall and the electron-atom collision frequencies decrease towards the thruster exit. The inequalities ν_{ew} , $\nu_{ea} << \nu_B$ are satisfied throughout the channel. In the real thruster, the neutral gas density decreases towards the channel exit due to ionization and the effective channel widening upon the transition from the annular to the cylindrical channel part. If a realistic neutral gas density profile was used in the simulations, ν_{ew} would become larger than ν_{ea} in the cylindrical part of the channel. However, in order to explain the observed discharge current, the anomalous collision frequency ν_B would have to remain much larger than both ν_{ew} and $\nu_{ea.}$

Even though the electron-wall collisions appear to have little effect on the electron cross-field transport, the electron-wall interaction is very important in terms of electron energy balance [40], [41]. For the parameters of Fig. 7, for example, the electron energy loss at the walls q_{ew} is equal to about 9.7 J/cm^3, while the energy loss due to inelastic electron-atom collisions q_{ea} is about 4.9 J/cm^3. q_{ew} and q_{ea} both decrease towards the channel exit and have values comparable with each other. The conclusions concerning the electron cross-field transport seem, however, to be insensitive to the details of the electron energy balance.

V. RECENT EXPERIMENTAL RESULTS AND PLANS FOR FUTURE WORK

The effect of the magnetic field on the discharge characteristics and efficiency of the low-power CHTs with channel outer diameters of 2.6 cm and 3 cm was investigated recently [25], [42]. In this section, we briefly describe a few interesting results obtained in these experiments. The observed effects (even though the underlying physics remains largely unexplored) have important implications for the problem of electron cross-field transport and suggest the directions for further studies.

The variation of the current in the back magnetic coil of the CHT mainly changes the magnetic field magnitude without altering the shape of magnetic field surfaces. It is generally observed that the increase of the back coil current leads to the monotonic decrease of the discharge current. The variation of the front coil current changes the shape of the magnetic field surfaces, with the most pronounced changes occurring in the cylindrical part of the channel. When the current in the front coil is counter-directed to that in the back coil ($I_{front}<0$), the "cusp" magnetic field with an enhanced radial component is created (see Fig. 2). Swapping the polarity of the front coil current ($I_{front}>0$) leads to the enhancement of the axial component of the magnetic field and generation of a stronger magnetic mirror near the thruster axis. The goal of the performed experiments was to investigate the dependence of the discharge current and generated thrust on the current in the front magnetic coil.

The experiments were performed in the Electric Propulsion and Plasma Dynamics Laboratory (EPPDyL) at Princeton University [43]. The operating background pressure of xenon in the EPPDyL vacuum facility was about one order of magnitude smaller than that in the Small Hall Thruster facility at PPPL. Importantly, it was observed that the magnetic field configuration

that minimizes the discharge current depends on the background gas pressure in the tank. In Fig. 9, the variation of the discharge current I_d with the current in the front coil I_{front} is shown for the EPPDyL and PPPL facilities. All discharge parameters are the same (anode flow rate μ=0.4 mg/s, U_d=250 V, I_{back}=+3 A), except for the background xenon pressure, which is about 6×10^{-6} Torr for the EPPDyL tank and 7×10^{-5} Torr for the PPPL tank. In the experiments at EPPDyL, when the background gas pressure in the near-filed thruster plume was raised by increasing xenon flow rate to the cathode, the values $I_d(I_{front})$ were found to shift closer to those corresponding to the PPPL conditions. It is important to emphasize, however, that electrons in the plume plasma are collisionless in both the PPPL and EPPDyL facilities: The electron mean free path is about the size of the tank, which is much larger than the thruster dimensions.

It is clear form Fig. 9 that the cusp magnetic field configuration minimizes the discharge current at high background pressure, while the direct configuration does the same at low pressure. Now, at low background pressure, the increase of I_{front} above ~ +1 A leads to the negligible variation of the discharge current. The decrease of I_{front}, on the contrary, brings about a rather sharp increase of I_d. Along with it, as the magnetic field configuration is changed from direct to cusp, the generated thrust slightly decreases (See Fig. 10). Consequently, in the voltage range from 200 to 300 Volts, the anode efficiency in the direct configuration is approximately factor of 1.5-1.7 larger than that in the cusp configuration.

The fact that the discharge current decreases with the increase in I_{front} (see Fig. 10) implies that the electron transport to the anode is suppressed more strongly in the direct magnetic field configuration than in the cusp configuration. Indeed, from the data shown in Fig. 10 it follows that

$$I_i^c \sim 0.95 I_i^d \sqrt{\varepsilon^d / \varepsilon^c}\,, \tag{3.a}$$

$$I_d^c \sim 1.37 I_d^d\,. \tag{3.b}$$

Here I_i is the ion current, ε is the mean ion energy, and superscripts "d" and "c" refer to the direct and cusp polarities, respectively. From Eqs. (3) we obtain the ratio of the electron currents in the cusp and direct configurations:

$$\frac{I_e^c}{I_e^d} \approx 1.37 + \frac{I_i^d}{I_e^d}\left(1.37 - 0.95\sqrt{\frac{\varepsilon^d}{\varepsilon^c}}\right). \tag{4}$$

When the thruster magnetic field configuration is changed, it is very unlikely that the average ion energy varies by more than about factor of 2. Thus, the ratio I_e^c / I_e^d is about 1.3 – 1.5.

The fact that the electron current in the direct configuration is smaller does not necessarily imply that the rate of electron cross-field transport is smaller. Plasma measurements, similar to those described in Sec. II, are required to understand how the magnetic field configuration and background gas pressure influence the electron anomalous transport. Studying the dependence of the plasma parameters on the magnetic field and gas pressure is a subject of ongoing research.

VI. CONCLUSIONS

Scaling to low-power Hall thrusters requires the magnetic field to be increased inversely with length, as the thruster channel size is decreased. In a strong magnetic field of a low-power Hall thruster, the rate of electron cross-field diffusion, required to sustain the discharge, can differ from that in a Hall thruster operating in the conventional kilowatt or subkilowatt power range. Thus, understanding of the mechanisms of electron transport is essential for the development of higher efficiency low-power thrusters and for scaling to small sizes.

The conventional (annular) Hall thrusters become inefficient when scaled to small sizes because of the large surface-to-volume ratio and the difficulty in miniaturizing the magnetic circuit. Also, the erosion of the walls of a small annular channel can severely limit the thruster lifetime. An alternative approach, which may be more suitable for scaling to low power, is a cylindrical Hall thruster (CHT). The 9 cm CHT, operated in the subkilowatt power range, and the miniature 2.6 cm and 3 cm CHT, operated in the power range 50–300 W, exhibit performance comparable with the conventional state-of-the-art annular Hall thrusters of the same size. Ion acceleration in the CHTs occurs mainly in the cylindrical part of the channel and beyond the thruster exit. Thus, CHTs, having lower surface-to-volume ratio as compared with conventional annular design Hall thrusters, should suffer lower erosion of the channel walls and, therefore, have a longer lifetime.

Plasma potential, ion density, and electron temperature profiles were measured inside the 2.6 cm cylindrical Hall thruster, operated in the vacuum facility with a relatively high background gas pressure ($< 10^{-4}$ Torr). The electron cross-field transport was studied for the typical operating regime. To analyze electron dynamics in the channel region of the 2.6 cm CHT, a Monte Carlo code was developed. The numerical model takes into account elastic and inelastic electron collisions with atoms, electron-wall collisions (backscattering, attachment, and

secondary electron emission), and Bohm diffusion. The comparison of numerical and experimental results shows that in order to explain the discharge current, observed in the 2.6 cm CHT, the electron anomalous collision frequency ν_B has to be high. As opposed to most of the conventional Hall thruster models, which predict the ratio ν_B/ω_c to be on the order of 10^{-2}, we find that in the 2.6 cm CHT ν_B has to be on the order of the Bohm value, $\nu_B \sim \omega_c/16$. The anomalous cross-field electron transport in the CHT is believed to be induced by high-frequency plasma instabilities. The EDF in a Hall thruster is depleted at high energy due to electron loss at the walls, thus indicating that the contribution of secondary electrons to cross-field transport is likely insignificant.

The effect of the magnetic field on the discharge current and generated thrust in the 2.6 cm and 3 cm CHTs was studied in the experiments performed at low background gas pressure ($< 10^{-5}$ Torr). These experiments demonstrated that the optimal regimes of thruster operation at low background pressure are, in fact, different from those at higher pressure. For instance, for both the 2.6 cm and 3 cm CHTs the discharge current decreases and the generated thrust slightly increases as the magnetic field configuration is changed from cusp to direct. This, most likely, implies that the electron transport to the anode is suppressed more strongly and the directionality of ion acceleration is better in the direct magnetic field configuration than in the cusp configuration. The thruster efficiency is accordingly larger in the direct configuration. Future experiments will address the question of how the rate of electron cross-field transport depends on the magnetic field configuration, channel geometric parameters, and the background gas pressure in the tank.

ACKNOWLEDGMENTS

The authors are grateful to Professor Edgar Choueiri for the provided opportunity to work with the EPPDyL thrust stand, and to Mr. Robert Sorenson for his assistance in the thrust measurements. This work was supported by grants from AFOSR, DARPA, and USDOE Contract AC02-76CH0-3073.

REFERENCES

1. I. Morozov and V. V. Savelyev, in *Review of Plasma Physic*s, vol. 21, p. 203, edited by B. B. Kadomtsev and V. D. Shafranov. Consultants Bureau, New York, 2000.
2. J. Mueller, in *Micropropulsion for Small Spacecraft, Progress in Astronautics and Aeronautics*, vol. 187, p. 45, edited by M.M. Micci and A.D. Ketsdever. AIAA Progress in Astronautics and Aeronautics, Reston, VA, 2000.
3. A. Fruchtman, "Limits on the efficiency of several electric thruster configurations", *Phys. Plasmas* vol. 10, no. 5, pp. 2100-2107, 2003.
4. G.S. Janes and R.S. Lowder, "Anomalous electron diffusion and ion acceleration in a low-density plasma", *Phys. Fluids*, vol. 9, no. 6, pp. 1115-1123, 1966.
5. A.I. Morozov and V.V. Savel'ev, "Theory of the near-wall conductivity", *Plasm. Phys. Rep.*, vol. 27, no. 7, pp. 570-575, 2001.
6. A.I. Bugrova, A.I. Morozov, and V.K. Kharchevnikov, "Eexperimental investigation of near wall conductivity", *Sov. J. Plasm. Phys.*, vol. 16, no. 12, pp. 849-856, 1990.
7. E. Fernandez and M.A. Cappelli, Bull. Am. Phys. Soc., vol. 45, no. 7, p. 166, 2000.

8. A. Cohen-Zur, A. Fructman, J. Ashkenazy, and A. Gany "Analysis of the steady-state axial flow in the Hall thruster", *Phys. Plasmas*, vol. 9, no. 10, pp. 4363-4374, 2002.
9. L. Dorf, V. Semenov, Y. Raitses, "Anode sheath in Hall thrusters", *Appl. Phys. Lett.*, vol. 83, no. 13, pp. 2551-2553, 2003.
10. S. Barral, K. Makowski, Z. Peradzynski, N. Gascon, and M. Dudeck, "Wall material effects in stationary plasma thrusters. II. Near-wall and in-wall conductivity", *Phys. Plasmas*, vol. 10, no. 10, 4137-4152, 2003.
11. E. Ahedo, J.M. Gallardo, and M. Martinez-Sanchez, "Effects of the radial plasma-wall interaction on the Hall thruster discharge", *Phys. Plasmas***,** vol. 10, no. 8, pp. 3397-3409, 2003.
12. M. Keidar, I.D. Boyd, and I.I. Beilis, "Plasma flow and plasma–wall transition in Hall thruster channel", *Phys. Plasmas*, vol. 8, no. 12, pp. 5315-5322, 2001.
13. J. Bareilles, G.J.M. Hagelaar, L. Garrigues, C. Boniface, J.P. Boeuf, and N. Gascon, "Critical assessment of a two-dimensional hybrid Hall thruster model: Comparisons with experiments", *Phys. Plasmas*, vol. 11, no. 6, 3035-3046, 2004.
14. J.M. Fife, Ph.D. thesis, Massachusetts Institute of Technology, 1998.
15. J.J. Szabo, Ph.D. thesis, Massachusetts Institute of Technology, 2001.
16. Y. Raitses, D. Staack, M. Keidar, and N.J. Fisch, "Electron-wall interaction in Hall thrusters", *Phys. Plasmas*, vol. 12, 057104, 2005.
17. O. Batishchev and M. Martinez-Sanchez, "Charged particles transport in the Hall effect thruster", IEPC 03-188, in Proc. 28th International Electric Propulsion Conference, Toulouse, France, 2003.
18. J.C Adam, A. Heron, G. Laval, "Study of stationary plasma thrusters using two-dimensional

fully kinetic simulations", *Phys. Plasmas*, vol. 11, no. 1, pp. 295-305, 2004.

19. L. Jolivet and J.F. Roussel, "Effects of the secondary electron emission on the sheath phenomenon in a hall thruster", in Proc. 3rd Spacecraft Propulsion Conference, pp. 367–376, Cannes, France, 1999.
20. N.B. Meezan and M.A. Cappelli, "Kinetic study of wall collisions in a coaxial Hall discharge", *Phys. Rev. E*, vol. 66, 036401, 2002.
21. N.B. Meezan, W.A. Hargus, and M.A. Cappelli, "Anomalous electron mobility in a coaxial Hall discharge plasma ", *Phys. Rev. E*, vol. 63, 026410, 2001.
22. M. Stanojevic, M. Cercek, T. Gyergyek, and N. Jelic, "Interpretation of a planar Langmuir probe current-voltage characteristic in a strong magnetic field", *Contrib. Plasma Phys.*, vol. 34, no. 5, pp. 607-633, 1994.
23. V. Khayms and M. Martinez-Sanches, in *Micropropulsion for Small Spacecraft, Progress in Astronautics and Aeronautics*, vol. 187, p. 45, edited by M.M. Micci and A.D. Ketsdever. American Institute of Aeronautics and Astronautics, Reston, VA, 2000.
24. Y. Raitses and N.J. Fisch, "Parametric investigations of a nonconventional Hall thruster", *Phys. Plasmas*, vol. 8, no. 5, pp. 2579-2586, 2001.
25. A. Smirnov, Y. Raitses, and N.J. Fisch, "Parametric investigation of miniaturized cylindrical and annular Hall thrusters", *J. Appl. Phys.*, vol. 92, no. 10, pp. 5673-5679, 2002.
26. A. Smirnov, Y. Raitses, and N.J. Fisch, "Enhanced ionization in the cylindrical Hall thruster", *J. Appl. Phys.*, vol. 94, no. 2, pp. 852-857, 2003.
27. A. Smirnov, Y. Raitses, and N.J. Fisch, "Plasma measurements in a 100 W cylindrical Hall thruster", *J. Appl. Phys.*, vol. 95, no. 5, pp. 2283-2292, 2004.
28. A. Smirnov, Y. Raitses, and N.J. Fisch, "Electron cross-field transport in a low power

cylindrical Hall thruster", *Phys. Plasmas*, vol. 11, no. 11, 4922-4933, 2004.

29. A. Smirnov, Y. Raitses, and N.J. Fisch, "The effect of magnetic field on the performance of low-power cylindrical Hall thrusters", IEPC paper 2005-099, to be presented at the 28th International Electric Propulsion Conference, Princeton, NJ, October 2005.
30. K.A. Polzin, T.E. Markusic, B.J. Stanojev, A. Dehoyos, Y. Raitses, A. Smirnov, and N.J. Fisch, "Performance of a low-power cylindrical Hall thruster", IEPC paper 2005-011, to be presented at the 28th International Electric Propulsion Conference, Princeton, NJ, October 2005.
31. H.R. Kaufman, R.S. Robinson, and R.I. Seddon, "End-Hall ion source", *J. Vac. Sci. Technol. A*, vol. 5, no. 4, pp. 2081-2084, 1987.
32. Field Precision, Albuquerque, NM. BStat 5.0. [Online]. Available: http://www.fieldp.com
33. J.P. Boris, in the Proc. Fourth Conf. Num. Sim. Plasmas, Naval Res. Lab, Washington, DC, pp. 3- 67, 2-3 Nov. 1970.
34. C.K. Birdsall, "Particle-in-cell charged-particle simulations, plus Monte Carlo collisions with neutral atoms, PIC-MCC", *IEEE Trans. Plasm. Sci.*, vol. 19, no. 2, pp. 65-85, 1991.
35. V. Yu. Fedotov, A.A. Ivanov, G. Guerrini, A.N. Vesselovzorov, and M. Bacal, "On the electron energy distribution function in a Hall-type thruster", *Phys. Plasmas*, vol. 6, no. 11, pp. 4360-4365, 1999.
36. J.P. Boeuf, E. Marode, "Monte Carlo analysis of an electron swarm in a nonuniform field: the cathode region of a glow discharge", *J. Phys. D*, vol. 15, no. 11, pp. 2169-2189, 1982.
37. A. Smirnov, Y. Raitses, and N.J. Fisch, "Electron transport and ion acceleration in a low-power cylindrical Hall thruster", AIAA paper 2004-4103, in Proc. 40th IAA/ASME/SAE/ ASEE Joint Propulsion Conference, Fort Lauderdale, Florida, 2004.

38. D. Bohm, in *The Characteristics of Electrical Discharges in Magnetic Fields*, chap. 2, p. 65, edited by A. Guthrie and R.K. Wakerling. McGraw-Hill, New York, 1949.

39. E.Y. Choueiri, "Plasma oscillations in Hall thrusters", *Phys. Plasmas*, vol. 8, no. 4, pp. 1411-1426, 2001.

40. E.Y. Choueiri, "Fundamental difference between the two Hall thruster variants", *Phys. Plasmas*, vol. 8, no. 11, pp. 5025-5033, 2001.

41. Y. Raitses, D. Staack, A. Smirnov, and N.J. Fisch, "Space charge saturated sheath regime and electron temperature saturation in Hall thrusters", *Phys. Plasmas*, vol. 12, 073507, 2005.

42. Y. Raitses, A. Smirnov, and N.J. Fisch, "Cyindrical Hall thrusters", presented at the 15th Annual NASA/JPL/MSFC Advanced Space Propulsion Workshop, Pasadena, CA, 2004.

43. E. A. Cubbin, J. K. Ziemer, E. Y. Choueiri, and R. G. Jahn, "Pulsed thrust measurements using laser interferometry", *Rev. Sci. Instrum.*, vol. 68, no. 6, pp. 2339-2346, 1997 .

Figure Captions

Fig. 1. (a) Schematic of a cylindrical Hall thruster. (b) The 2.6 cm cylindrical Hall thruster.

Fig. 2. (a) Magnetic field profiles in the 2.6 cm CHT. I_{back} = 2.5A, I_{front} = -1A. Dashed lines at z=6 mm and z=22 mm show the edge of the annular channel part and the thruster exit, respectively. (b) Probe setup used in the experiments. Magnetic field distribution is given for the same coil currents as in Fig 2(a). Illustrative electron trajectory in the cylindrical part of the channel is indicated, and hybrid mechanism of electron trapping is schematically shown. μ_e is the electron magnetic moment.

Fig. 3. Electron temperature (a), plasma potential (b), and plasma density (c) profiles in the 2.6 cm CHT [28]. Dashed lines at z=6 mm and z=22 mm show the edge of the annular channel part and the thruster exit, respectively. In (a) and (b), Y-axis error bars represent the entire statistical spread of the measured data. For plasma density measurements near the outer channel wall (c), only the intervals, in which the real values of the plasma density are located, can be given.

Figure 4. (a) Plasma potential profile along the outer channel wall, measured (symbols) and "tailored" (line). Between the measurement points, plasma potential $\phi(z,R)$ is assumed to be proportional to magnetic flux function $\psi(z,R)$. (b) Distribution of the "tailored" plasma potential in the channel.

Fig. 5. Distributions of the electron density (a) and the effective electron temperature (b) in the channel of the 2.6 cm CHT. The solid dark rectangle in the lower left-hand side corner of the pictures ($0<z<6$, $0<R<7$) represents the cross section of the central ceramic piece.

Fig. 6. Calculated profiles of the plasma density at the outer channel wall between z=5 mm and 13.5 cm locations for different values of κ_B. The uncertainty bars represent the results of the plasma density measurements.

Fig. 7. Typical electron distribution function (EDF) in the annular part of the channel. T_{bulk} and T_{tail} are obtained by fitting the corresponding parts of the EDF with linear functions.

Fig. 8. Simulated values of N_e at z=5 mm near the outer wall versus Bohm parameter κ_B. Solid line shows the result of fitting the simulated data with function A/κ_B.

Fig. 9. The dependences of the discharge current on the current in the front magnetic coil in the 2.6 cm CHT for the EPPDyL and PPPL facilities. All discharge parameters are the same (anode flow rate μ=0.4 mg/s, U_d=250 V, I_{back}=+3 A), except for the background gas pressure, which is equal to 6.3×10^{-6} Torr for the EPPDyL tank and 6.7×10^{-5} Torr for the PPPL tank.

Fig. 10. The dependencies of the discharge current and thrust on the front coil current in the 2.6 cm CHT operated in the EPPDyL facility (background gas pressure ~ 6×10^{-6} Torr). Anode and

cathode xenon flow rates are 4 sccm and 2 sccm, respectively; I_{back} = 3A. $I_{front}>0$ ($I_{front}<0$) corresponds to the direct (cusp) magnetic field configuration.

Fig. 1

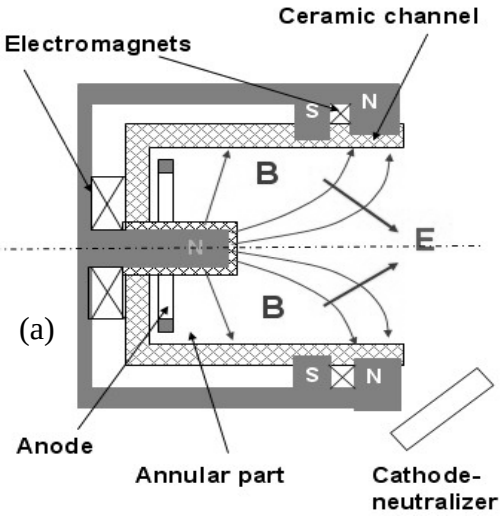
Ceramic channel
Electromagnets
S
N
B
E
B
(a)
S
N
Anode
Annular part
Cathode-
neutralizer

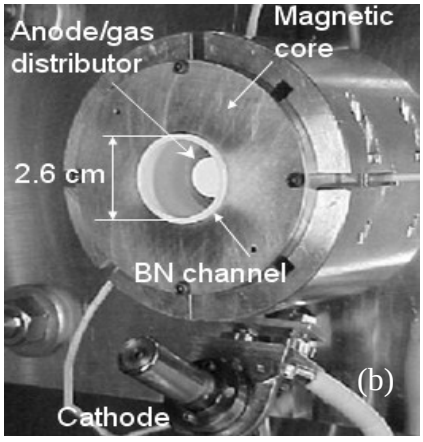
Anode/gas
distributor
Magnetic
core
2.6 cm
BN channel
(b)
Cathode

Fig. 2

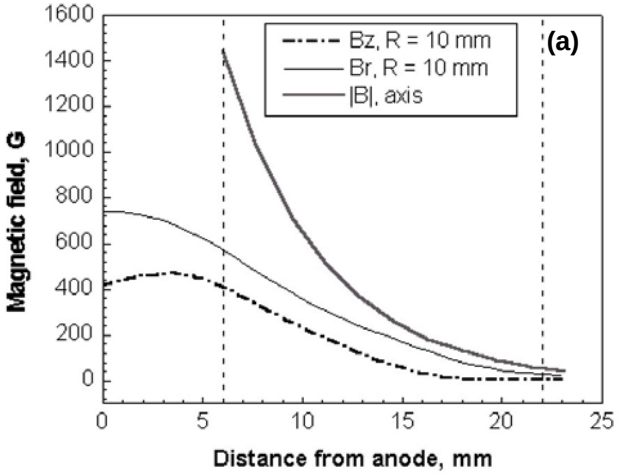
Bz, R = 10 mm
Br, R = 10 mm
|B|, axis
(a)
Magnetic field, G
Distance from anode, mm
1600
1400
1200
1000
800
600
400
200
0
0
5
10
15
20
25

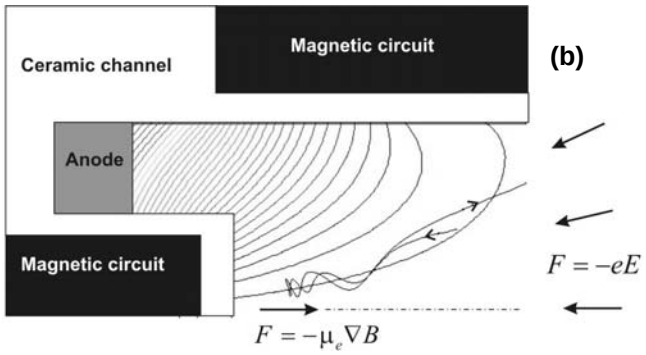
Ceramic channel
Magnetic circuit
(b)
Anode
Magnetic circuit
$F = -eE$
$F = -\mu_e \nabla B$

Fig. 3

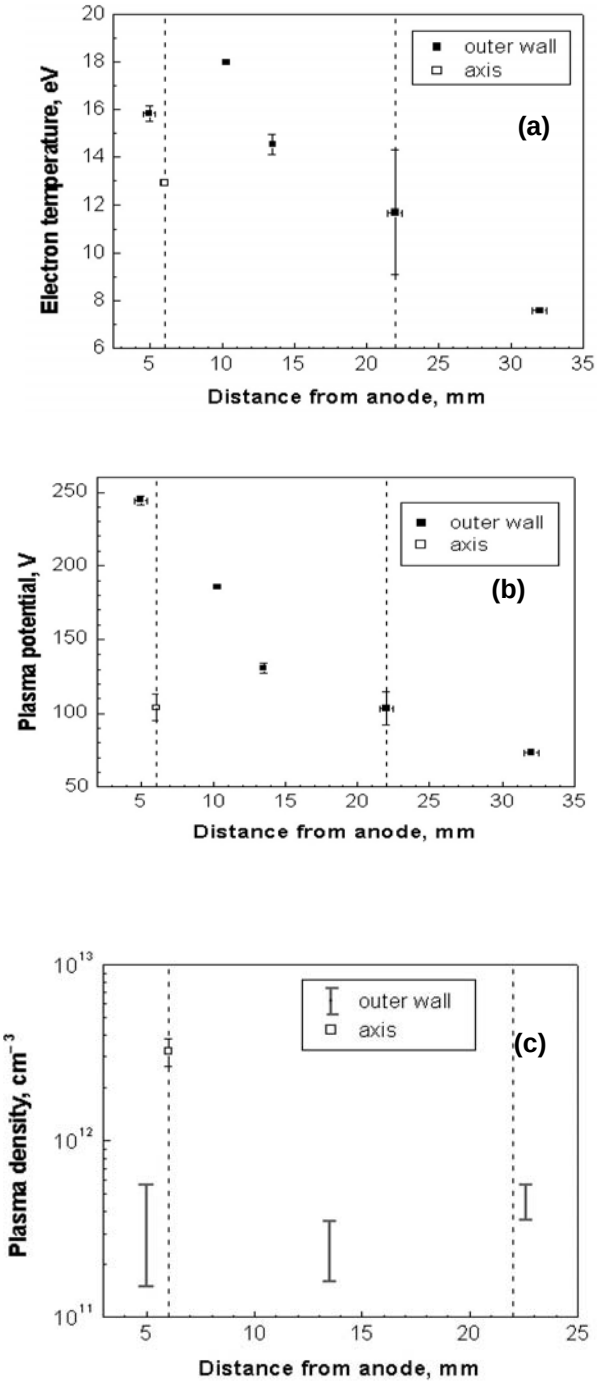
Electron temperature, eV
Distance from anode, mm
outer wall
axis
(a)
Plasma potential, V
Distance from anode, mm
outer wall
axis
(b)
Plasma density, cm^{-3}
Distance from anode, mm
outer wall
axis
(c)

Fig. 4

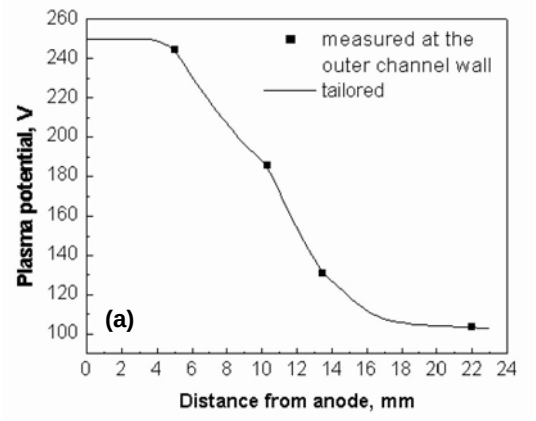
measured at the outer channel wall
tailored
Plasma potential, V
Distance from anode, mm
(a)

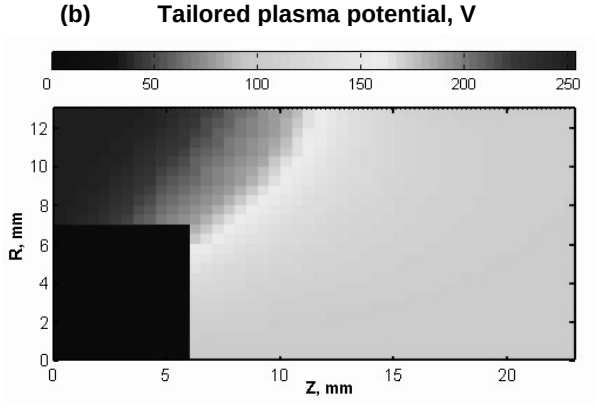
(b) Tailored plasma potential, V
R, mm
Z, mm

Fig. 5

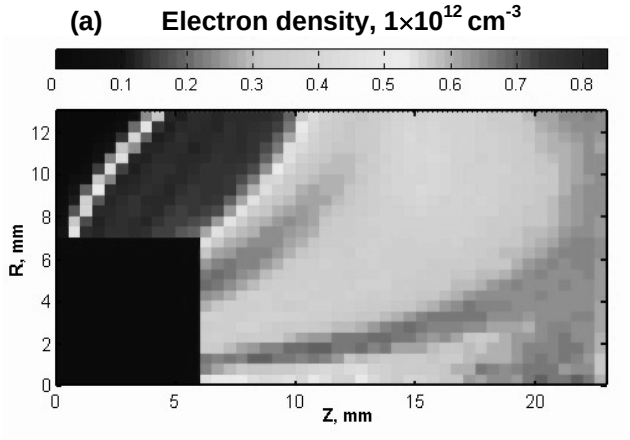
(a) Electron density, 1×10^12 cm^-3
0 0.1 0.2 0.3 0.4 0.5 0.6 0.7 0.8
R, mm
0 2 4 6 8 10 12
Z, mm
0 5 10 15 20

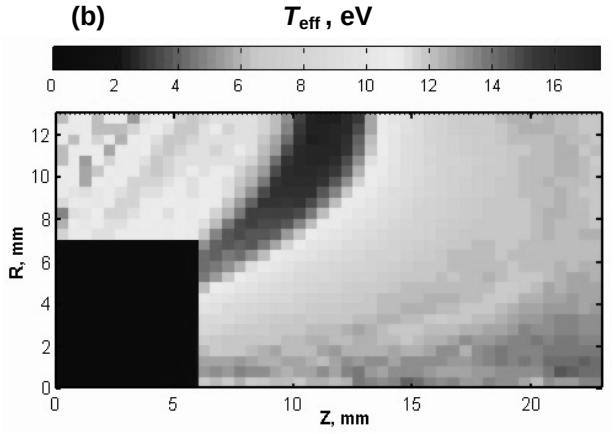
(b) T_eff , eV
0 2 4 6 8 10 12 14 16
R, mm
0 2 4 6 8 10 12
Z, mm
0 5 10 15 20

IEEE Trans. Plasma Science
A. Smirnov, Y. Raitses, N.J. Fisch.

Fig. 6

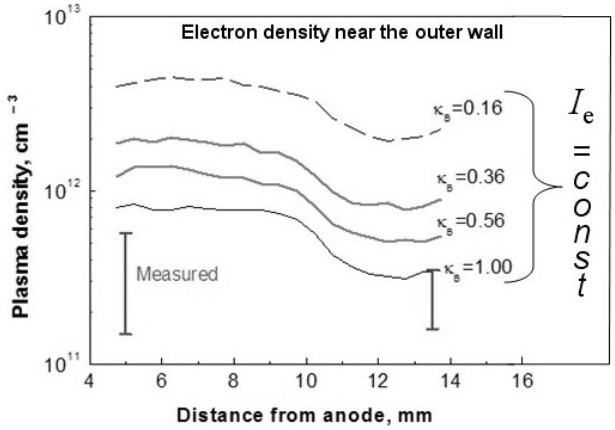

IEEE Trans. Plasma Science
A. Smirnov, Y. Raitses, N.J. Fisch.

Fig. 7

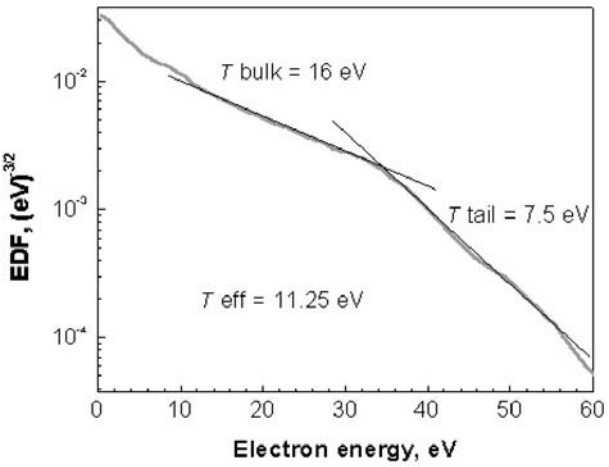

IEEE Trans. Plasma Science
A. Smirnov, Y. Raitses, N.J. Fisch.

Fig. 8

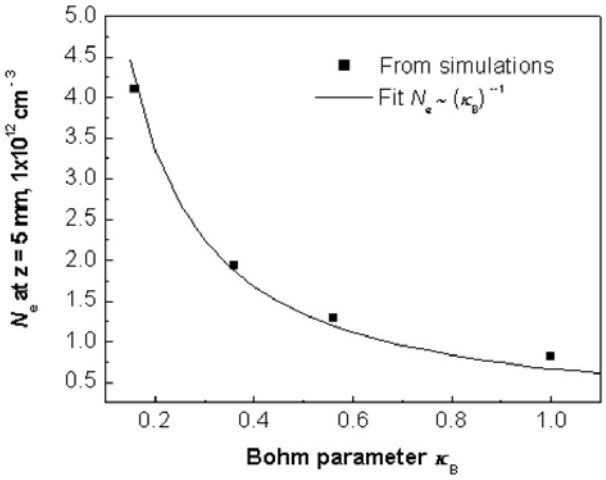

IEEE Trans. Plasma Science
A. Smirnov, Y. Raitses, N.J. Fisch.

Fig. 9

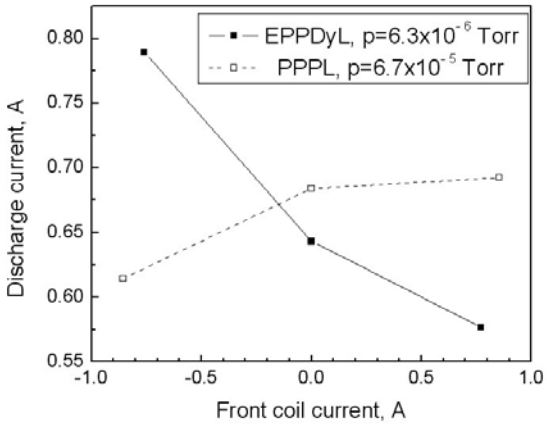

IEEE Trans. Plasma Science
A. Smirnov, Y. Raitses, N.J. Fisch.

Fig. 10

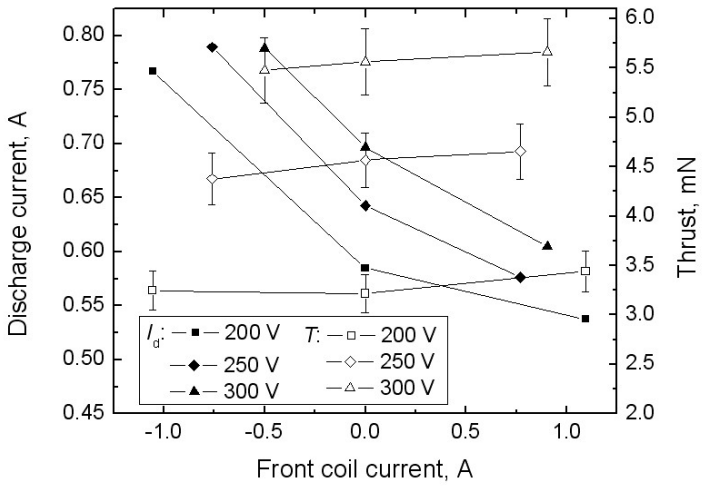

External Distribution

Plasma Research Laboratory, Australian National University, Australia
Professor I.R. Jones, Flinders University, Australia
Professor João Canalle, Instituto de Fisica DEQ/IF - UERJ, Brazil
Mr. Gerson O. Ludwig, Instituto Nacional de Pesquisas, Brazil
Dr. P.H. Sakanaka, Instituto Fisica, Brazil
The Librarian, Culham Science Center, England
Mrs. S.A. Hutchinson, JET Library, England
Professor M.N. Bussac, Ecole Polytechnique, France
Librarian, Max-Planck-Institut für Plasmaphysik, Germany
Jolan Moldvai, Reports Library, Hungarian Academy of Sciences, Central Research Institute for Physics, Hungary
Dr. P. Kaw, Institute for Plasma Research, India
Ms. P.J. Pathak, Librarian, Institute for Plasma Research, India
Dr. Pandji Triadyaksa, Fakultas MIPA Universitas Diponegoro, Indonesia
Professor Sami Cuperman, Plasma Physics Group, Tel Aviv University, Israel
Ms. Clelia De Palo, Associazione EURATOM-ENEA, Italy
Dr. G. Grosso, Instituto di Fisica del Plasma, Italy
Librarian, Naka Fusion Research Establishment, JAERI, Japan
Library, Laboratory for Complex Energy Processes, Institute for Advanced Study, Kyoto University, Japan
Research Information Center, National Institute for Fusion Science, Japan
Professor Toshitaka Idehara, Director, Research Center for Development of Far-Infrared Region, Fukui University, Japan
Dr. O. Mitarai, Kyushu Tokai University, Japan
Mr. Adefila Olumide, Ilorin, Kwara State, Nigeria
Dr. Jiangang Li, Institute of Plasma Physics, Chinese Academy of Sciences, People's Republic of China
Professor Yuping Huo, School of Physical Science and Technology, People's Republic of China
Library, Academia Sinica, Institute of Plasma Physics, People's Republic of China
Librarian, Institute of Physics, Chinese Academy of Sciences, People's Republic of China
Dr. S. Mirnov, TRINITI, Troitsk, Russian Federation, Russia
Dr. V.S. Strelkov, Kurchatov Institute, Russian Federation, Russia
Kazi Firoz, UPJS, Kosice, Slovakia
Professor Peter Lukac, Katedra Fyziky Plazmy MFF UK, Mlynska dolina F-2, Komenskeho Univerzita, SK-842 15 Bratislava, Slovakia
Dr. G.S. Lee, Korea Basic Science Institute, South Korea
Dr. Rasulkhozha S. Sharafiddinov, Theoretical Physics Division, Insitute of Nuclear Physics, Uzbekistan
Institute for Plasma Research, University of Maryland, USA
Librarian, Fusion Energy Division, Oak Ridge National Laboratory, USA
Librarian, Institute of Fusion Studies, University of Texas, USA
Librarian, Magnetic Fusion Program, Lawrence Livermore National Laboratory, USA
Library, General Atomics, USA
Plasma Physics Group, Fusion Energy Research Program, University of California at San Diego, USA
Plasma Physics Library, Columbia University, USA
Alkesh Punjabi, Center for Fusion Research and Training, Hampton University, USA
Dr. W.M. Stacey, Fusion Research Center, Georgia Institute of Technology, USA
Director, Research Division, OFES, Washington, D.C. 20585-1290

The Princeton Plasma Physics Laboratory is operated
by Princeton University under contract
with the U.S. Department of Energy.

Information Services
Princeton Plasma Physics Laboratory
P.O. Box 451
Princeton, NJ 08543

Phone: 609-243-2750
Fax: 609-243-2751
e-mail: pppl_info@pppl.gov
Internet Address: http://www.pppl.gov